

# Two Structural Subdomains of Barstar Detected by Rapid Mixing NMR Measurement of Amide Hydrogen Exchange

Abani K. Bhuyan and Jayant B. Udgaonkar\*

National Centre for Biological Sciences, Tata Institute of Fundamental Research, Bangalore, India

**ABSTRACT** Equilibrium amide hydrogen exchange studies of barstar have been carried out at pH 6.7, 32°C using one- and two-dimensional nuclear magnetic resonance. An unusually large fraction of the backbone amide hydrogens of barstar exchange too fast to be measured, and the exchange rates of only fifteen slow-exchanging amide sites including indole amides of two tryptophans could be measured in the presence of 0 to 1.8 M guanidine hydrochloride (GdnHCl). Measurement of exchange occurring in tens of seconds in the unfolding transition region was possible by the use of a fast stopped-flow mixing method. The observed exchange rates have been simulated in the EX2 limit according to a two-process model that incorporates two exchange-competent states: a transiently unfolded state ( $U^*$ ) in which many amide hydrogens are completely accessible to solvent-exchange, and a near-native locally unfolded state ( $N^*$ ), in which only one or a few amide hydrogens are completely accessible to solvent-exchange. The two-process model appears to account for the observed exchange behavior over the entire range of GdnHCl concentrations studied. For several measurable slow-exchanging amide hydrogens, the free energies of production of exchange-competent states from the exchange-incompetent native state are significantly higher than the free-energy of production of the equilibrium unfolded state from the native state, when the latter is determined from circular dichroism- or fluorescence-monitored equilibrium unfolding curves. The result implies that  $U^*$ , which forms transiently in the strongly native-like conditions used for the hydrogen exchange studies, is higher in energy than the equilibrium-unfolded state. The higher energy of this transiently unfolded exchange-competent state can be attributed to either proline isomerization or to the presence of residual structure. On the basis of the free energies of production of exchange-competent states, the measured amide sites of barstar appear to define two structural subdomains—a three-helix unit

and a two- $\beta$ -strand unit in the core of the protein. **Proteins 30:295–308, 1998.** © 1998 Wiley-Liss, Inc.

**Key words:** hydrogen exchange mechanism; denaturants

## INTRODUCTION

Hydrogen exchange has long been recognized as a powerful approach in protein and nucleic acid research.<sup>1</sup> The objectives of exchange measurement include investigation of molecular structure, motions, and energetics of conformational interconversions as well as understanding the physical mechanism of hydrogen exchange. Hydrogen exchange methods have been invaluable in structural description of protein folding intermediates,<sup>2–4</sup> characterization of non-native compact protein states,<sup>5</sup> detection of structural and allosteric changes in proteins,<sup>6</sup> and identification of motional domains important in protein folding.<sup>7–9</sup> In spite of such major practical advances, a number of issues are poorly understood: 1) the coherence of exchange of a given set of amides, 2) factors responsible for enhancing or blocking exchange in a protein segment, 3) the importance of local fluctuations, and 4) the relationship between local and global unfolding motions. These issues form the current focus of hydrogen exchange studies.<sup>10–13</sup>

The exchange behavior of protein amide hydrogens in very mild denaturing conditions has been measured for only a few proteins.<sup>14–17</sup> In this article,

*Abbreviations:* HX, hydrogen exchange; CD, circular dichroism; GdnHCl, guanidine hydrochloride; TOCSY, total correlation spectroscopy; BPTI, bovine pancreatic trypsin inhibitor; LEM, linear free-energy model; N, native state;  $N^*$ , an ensemble of near-native states;  $U^*$ , transiently unfolded state in which many amide hydrogens are fully accessible to solvent; U, equilibrium unfolded state;  $\Delta G_{op}$ , the free-energy of production of exchange-competent states ( $N^* + U^*$ ) from the exchange-incompetent N state.

Contract grant sponsor: Tata Institute of Fundamental Research; Contract grant sponsor: Department of Biotechnology, Government of India.

\*Correspondence to: Prof. Jayant Udgaonkar, National Centre for Biological Sciences, TIFR Centre, PO Box 1234, Indian Institute of Science Campus, Bangalore 560012, India.

E-mail: jayant@ncbs.tifrbng.res.in

Received 8 April 1997; Accepted 28 August 1997

hydrogen exchange properties of some backbone amides of barstar in the native and near-native states in the presence of low to substantially denaturing concentrations of guanidine hydrochloride is reported. Barstar, an 89-amino acid monomeric protein, is a ribonuclease inhibitor produced intracellularly by the bacterium *Bacillus amyloliquefaciens*.<sup>18</sup> Several reports on stability, chain folding and unfolding, internal packing, and motional dynamics of barstar have appeared (reviewed in ref. 19).

The availability of complete proton resonance assignment<sup>20,21</sup> (unpublished result from this laboratory) and the restrained minimized mean structure of barstar in solution<sup>21</sup> facilitated the present hydrogen exchange measurements. It is argued here that the equilibria for local fluctuational motions are only marginally sensitive to the presence of denaturant. For several amide sites, the free energies of conversion of the exchange-incompetent native state to exchange-competent states have been found to be higher than the free energy of equilibrium unfolding of barstar. On the basis of hydrogen exchange behavior, two structural subdomains of barstar have been identified: one formed of helices 1, 2, and 4, and the other defined by a close association of  $\beta$  strands 2 and 3.

## MATERIALS AND METHODS

Overexpression and purification of barstar have been described previously.<sup>22</sup> D<sub>2</sub>O and H<sub>2</sub>O buffer solutions contained 20 mM sodium phosphate at pH 6.7, 32°C. The reported pH of the D<sub>2</sub>O buffer is the uncorrected pH meter reading. GdnHCl (Sigma Chemical Co., St. Louis, MO) was deuterated by repeated lyophilization of its D<sub>2</sub>O solution. Buffer components, acids and bases, and other chemicals were reagent grade.

GdnHCl-induced equilibrium unfolding in H<sub>2</sub>O and D<sub>2</sub>O solutions was monitored by CD (222 nm) and fluorescence. For CD measurement, a Jasco J720 spectropolarimeter was used. Fluorescence measurements were performed in a photon counting instrument (SPEX 320) with the excitation (287 nm) and emission (320 nm) slits set at 0.5 and 1.25 nm, respectively. The protein solutions used for equilibrium experiments were equilibrated at room temperature for about 4 hours before measurement.

To initiate proton-to-deuterium exchange of amides two approaches were employed. In the first method, applicable for exchange studies in lower concentration of denaturants, ~0.65 ml of an aqueous solution of the native protein (typically 1.5 mM dissolved in 20 mM phosphate buffer at pH 6.7) was passed through a 5 cm  $\times$  1.25 cm Sephadex G25 column equilibrated with the D<sub>2</sub>O buffer containing a desired concentration of guanidine hydrochloride. The typical run time for H<sub>2</sub>O to D<sub>2</sub>O solvent ex-

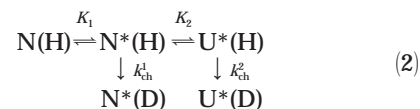
change was 45 seconds. "Zero time" of exchange was counted as soon as the eluate was collected. The period between the "zero time" and starting the first NMR spectrum (~4–6 minutes) defines the dead time. The second method (details to be published elsewhere) was suitable for measurement under substantially denaturing conditions (0.8–1.8 M GdnHCl in this study) where HX takes place in tens of seconds to a few minutes. One part of a 15 mM protein solution prepared in the aqueous buffer and nine parts of the deuterated buffer containing a desired concentration of GdnHCl were injected simultaneously into the NMR tube with the help of plastic transfer lines reaching the probe. To ensure thermal equilibration before mixing, the solution-filled flow lines were allowed to hang within the magnet for 5 minutes at 32°C before injection. A mixing time of about 2–3 seconds is estimated. The time delay between sample injection and acquiring the first FID was typically 6 seconds. 1D spectra were acquired in arrayed mode with no preacquisition delay. 1D and 2D NMR spectra were recorded using a 500 MHz (Bruker AMX 500) or a 600 MHz (Varian Unity Plus) spectrometer using a spectral width of 8000 Hz. 1D spectra were of 16K data points (8K when arrayed). TOCSY spectra were recorded with a 30 ms mixing time, 260 t1, and 2048 t2. Residual water was suppressed by presaturation. Data were processed using UXNMR (Bruker), Vnmr (Varian), and Felix softwares.

Hydrogen exchange rates were determined from the observed decay of resonance intensities according to equation (1):

$$I(t) = I_{\infty} + A \exp(-k_{\text{ex}}^{\text{obs}} t) \quad (1)$$

where  $I_{\infty}$  is the steady-state intensity at infinite time,  $A$  is the total change in intensity (i.e., the intensity at "zero time" minus  $I_{\infty}$ ), and  $k_{\text{ex}}^{\text{obs}}$  is the observed rate of hydrogen exchange. The inaccuracy in intensity measurement was  $\pm 5\%$ , but rose to approximately  $\pm 12\%$  for some of the transient mixing data.

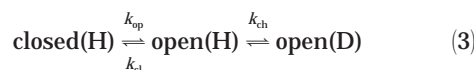
The GdnHCl-dependence of the free energy of production of HX competent states,  $\Delta G_{\text{op}}$ , was analyzed on the basis of the "two-process" model,<sup>23,24</sup> in which exchange can occur via local as well as global unfolding reactions. The two-process model can be formalized in the following equation:



where N, N\*, and U\*, respectively, are the native, near-native, and transiently unfolded states of the protein. N\*, which is structurally similar to N,

represents an ensemble of locally unfolded forms in each of which one or a few amide sites are fully exposed to solvent.  $U^*$  represents a transiently unfolded form in which many amide sites are fully exposed to solvent. A unique  $N^*$  state may occur for each amide site. An individual amide hydrogen can become exchange-competent when  $N$  fluctuates locally to  $N^*$  and/or  $N^*$  transiently unfolds to  $U^*$ .  $K_1$  ( $=N^*/N$ ) and  $K_2$  ( $=U^*/N^*$ ) define the two structure-opening equilibria.  $k_{ch}^1$  and  $k_{ch}^2$  are chemical exchange rates of the amide proton in  $N^*$  and  $U^*$ , respectively. A standard procedure is available for computation of  $k_{ch}^2$  only,<sup>25</sup> and to model the present experimental data it has been assumed that  $k_{ch}^1 = k_{ch}^2$  on the expectation that a particular amide site is as solvent-exposed in  $N^*$  as in  $U^*$ . This assumption was not made in the original two-process model.

The  $N$  state of equation (2) is identified with the closed state, and the  $N^*$  and  $U^*$  states are identified with the open state in the Linderström-Lang mechanism for hydrogen exchange.<sup>1,26</sup>



where  $k_{op}$  and  $k_{cl}$  are the rate constants for opening and closing of an amide site, and  $k_{ch}$  is the exchange rate of the same amide proton in a random polypeptide.<sup>25</sup>

Exchange occurs by the EX2 mechanism when  $k_{cl} \gg k_{ch}$ . In the EX2 limit, the equilibrium constant defining the equilibrium between the exchange-incompetent closed form and the exchange-competent open form,  $K_{op}$  ( $=k_{op}/k_{cl}$ ) is determined by the two experimentally determined exchange rate constants,  $k_{ex}^{obs}$  (equation 1) and  $k_{ch}$ :<sup>25</sup>

$$\frac{k_{ex}^{obs}}{k_{ch}} = \frac{K_{op}}{1 + K_{op}} \quad (4)$$

When, in addition,  $k_{cl} \gg k_{op}$ , (this condition is also frequently included in the definition of the EX2 limit) so that  $K_{op} \ll 1$ , equation (4) reduces to equation (5):

$$\frac{k_{ex}^{obs}}{k_{ch}} = K_{op} = \frac{1}{P} \quad (5)$$

where  $P$  is defined as the protection factor for exchange.

When two exchange-competent forms are present as in equation (2),  $K_{op}$  is given by:

$$K_{op} = \frac{N^* + U^*}{N} = K_1(1 + K_2). \quad (6)$$

In the EX2 limit,  $K_{op}$  for equation (2) is also experimentally determined by the use of equation (5), as described above.

The free energy of production of exchange-competent states ( $N^* + U^*$ ) from the exchange-incompetent state ( $N$ ) is determined by the use of equation (7):

$$\Delta G_{op} = -RT \ln K_{op} = -RT \ln \frac{k_{ex}^{obs}}{k_{ch}} \quad (7)$$

If, for the scheme depicted in equation (2),  $U^*$  is taken to be equivalent to  $U$ , the equilibrium unfolded state, then  $K_u$ , the equilibrium constant defining the global unfolding of  $N$  and  $N^*$  is given by:

$$K_u = \frac{U}{N + N^*} = \frac{K_2 K_1}{1 + K_1} \quad (8)$$

$K_u$  is experimentally determined from GdnHCl-induced equilibrium unfolding experiments in which unfolding is monitored by fluorescence or far-UV CD, which do not distinguish between  $N$  and  $N^*$ .

Combining equations (6) and (8) yields equation (9):

$$\Delta G_{op} = -RT \ln [K_1 + K_u(1 + K_1)]. \quad (9)$$

The analysis of  $\Delta G_{op}$  as a function of GdnHCl therefore requires the knowledge of denaturant-dependent behavior of the two equilibrium constants  $K_1$  and  $K_u$ . We assume here that  $K_1$  has no significant dependence on GdnHCl concentration (see the Discussion section). From the linear free-energy model of denaturant-dependence of global unfolding, found to be valid for a large number of proteins,<sup>27,28</sup> including barstar,<sup>29</sup>  $K_u$  and  $\Delta G_u$  are expressed as

$$K_u = K_u^{\circ} \exp \frac{m[\text{GdnHCl}]}{RT} \quad (10)$$

$$\Delta G_u = \Delta G_u^{\circ} + m[\text{GdnHCl}] \quad (11)$$

where  $K_u^{\circ}$  and  $\Delta G_u^{\circ}$  are the equilibrium constant and change in free energy, respectively, for the  $N \rightleftharpoons U$  reaction in water, and  $m$  is related to denaturant-binding surface area exposed upon unfolding. With this expression for  $K_u$ , equation (9) can be rewritten as

$$\Delta G_{op} = -RT \ln \left[ K_1 + K_u^{\circ} \exp \frac{m[\text{GdnHCl}]}{RT} (1 + K_1) \right] \quad (12)$$

This equation, which predicts a nonlinear dependence of  $\Delta G_{op}$  at lower concentrations of GdnHCl, is the same as the one previously derived by Qian and coworkers<sup>30</sup> with a near-native exchange competent species off the pathway from N to U\*. It should be emphasized that hydrogen exchange studies cannot distinguish an on-pathway role for N\* from an off-pathway role.

In the global unfolding transition zone, where the values of  $K_u$  lie between 0.1 and 10,  $K_u$  is much larger in value than  $K_1$ , which has GdnHCl concentration-independent values in the range  $10^{-4}$  to  $10^{-5}$  for different amide hydrogens. Thus, equation (12) reduces to equation (13), in which  $\Delta G_{op}$  equals  $\Delta G_u$ :

$$\Delta G_{op} = -RT \ln \left[ K_u^{\circ} \exp \frac{m[\text{GdnHCl}]}{RT} \right]. \quad (13)$$

## RESULTS

Figure 1 shows the fingerprint regions of the TOCSY spectra of barstar recorded at different times after hydrogen-to-deuterium exchange was initiated in the absence of GdnHCl. Only  $\sim 30$  resonances are observed in the earliest recorded spectrum (Fig. 1A) indicating that amide protons of most of the residues exchange out within the dead time of measurement. More interestingly, two-thirds of the resonances observable after 5 minutes disappear in about 100 minutes (Fig. 1A,C). After 340 minutes, virtually all amide protons have exchanged out.

By combining 1D and 2D spectra it was possible to determine the exchange kinetics of thirteen backbone amide sites and the indole protons ( $\epsilon_1\text{NH}$ ) of *W38* and *W44* in GdnHCl concentrations from 0 to 1.8 M. Figure 2A represents the observed exchange kinetics of amide protons from five residues in the presence of 0.33 M GdnHCl. Non-zero values of  $I_{ex}$  [Eq. (1)] are observed because of the presence of residual water in the samples. Exchange rates of all the measured main-chain hydrogens are found to be sensitive to the added concentration of the denaturant. The exchange kinetics in the presence of increasing concentration of GdnHCl are illustrated for *K78* in Figure 2B. The rate increases from  $1.12 \text{ h}^{-1}$  in the native state to  $18.3 \text{ h}^{-1}$  when exchange is allowed in the presence of 0.73 M GdnHCl.

GdnHCl-induced equilibrium unfolding curves of barstar in  $\text{H}_2\text{O}$  and  $\text{D}_2\text{O}$  solutions are presented in Figure 3. Far-UV CD were used to monitor unfolding. Some proteins are known to be more stable in  $\text{D}_2\text{O}$  than in  $\text{H}_2\text{O}$ . The equilibrium unfolding data in Figure 3, measured in both  $\text{D}_2\text{O}$  and  $\text{H}_2\text{O}$  solutions indicate that barstar gains no extra stability in  $\text{D}_2\text{O}$ . The values for  $\Delta G_u^{\circ}$  and  $m$  determined here,  $5.4 \pm 0.5$

$\text{kcal mol}^{-1}$  and  $-2.8 \pm 0.2 \text{ kcal mol}^{-1} \text{ M}^{-1}$ , respectively, in  $\text{H}_2\text{O}$ , and  $5.0 \pm 0.5 \text{ kcal mol}^{-1}$  and  $-2.6 \pm 0.2 \text{ kcal mol}^{-1} \text{ M}^{-1}$ , respectively, in  $\text{D}_2\text{O}$ , are consistent with previously published values measured using optical techniques.<sup>31,32</sup>

Figure 4 illustrates the GdnHCl-dependencies of  $\Delta G_{op}$  for some of the measured amide protons of barstar. Values of  $\Delta G_{op}$  were determined from NMR-measured  $k_{ex}^{obs}$  values in different GdnHCl concentrations by the use of equation (7). The solid lines represent simulations according to equation (12). The behavior of the  $\Delta G_{op}$  curves shown in Figure 4 can be summarized as the following:

1. For all measurable protons,  $\Delta G_{op}^{\circ}$  ranges from  $\sim 5.1 \text{ kcal mol}^{-1}$  (*V45*) to  $\sim 6.7 \text{ kcal mol}^{-1}$  (*L49*) (Fig. 4a,d). The small dispersion in  $\Delta G_{op}$  values observed for different protons under natively-like conditions narrows down as GdnHCl concentration increases through the pretransition to the transition region of equilibrium unfolding of barstar (Fig. 4). Denaturant-dependent dispersion in the HX curves indicates that at low concentration of GdnHCl a large number of structure-opening equilibria (i.e., a range of  $K_{op}$  values) are involved in the exchange of protein amide hydrogens.
2. In the presence of lower concentration GdnHCl, the  $\Delta G_{op}$  curves have smaller  $m$  values (shallow slopes) implying that local motions leading to hydrogen exchange do not produce significant exposure of buried surface. In spite of their association with small  $m$  values, the local fluctuations involve large  $\Delta G_{op}$  values for productive hydrogen exchange. Values obtained for  $K_1$  for individual amide hydrogens are in the range  $10^{-4}$  to  $10^{-5}$ . The shallowness of  $\Delta G_{op}$  curves decreases as the GdnHCl concentration increases in the exchanging medium. In the transition region of global unfolding (beyond  $\approx 1.0 \text{ M}$  GdnHCl) the slope of  $\Delta G_{op}$  curves for all protons,  $-2.7 \pm 0.1$ , matches the global  $m$  value ( $-2.8 \text{ kcal mol}^{-1} \text{ M}^{-1}$ ), suggesting that the protein surface exposed during hydrogen exchange is equal to the surface exposure associated with equilibrium global unfolding. Hence in this regime large amplitude motions similar to those responsible for global unfolding may be implicated in hydrogen exchange. For some amide hydrogens (see, for instance, *E8* and *L34* in Fig. 4), there appear to be discontinuities in the values of  $\Delta G_{op}$  at 1.0 M GdnHCl, where the global unfolding transition begins. The reason for these discontinuities is not known. While the fits of the data to equation (12) are reasonably good, it is possible that they would improve marginally if the values for  $k_{ch}^1$  and  $k_{ch}^2$  were not taken to be equal in equation (2), and if their dependencies on

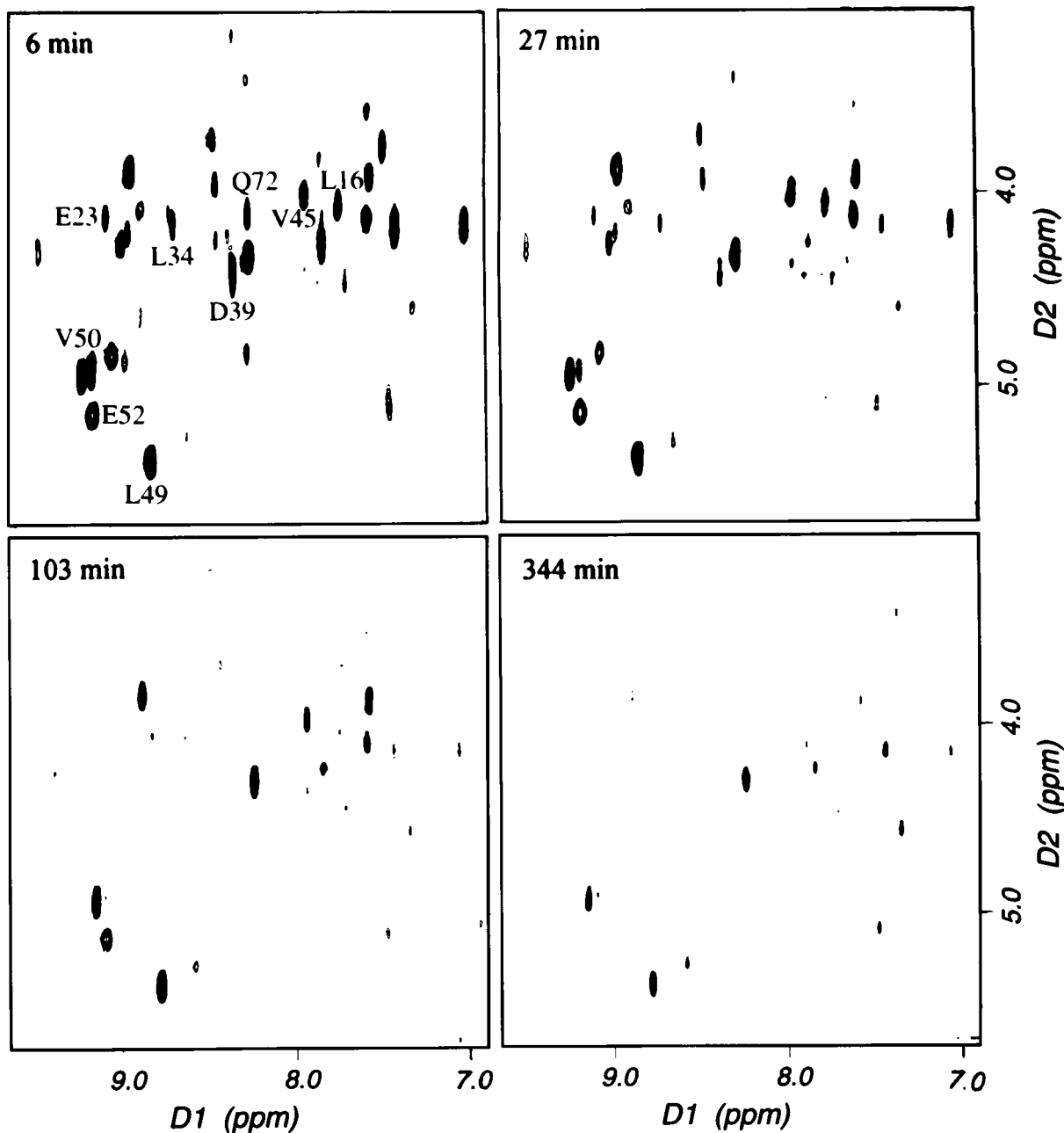


Fig. 1. Fingerprint regions of TOCSY spectra of native barstar in  $D_2O$  at pH 6.7, 32°C. The time lapse between  $H_2O$  to  $D_2O$  solvent exchange and recording the first spectrum is 6 minutes.

GdnHCl were corrected for. The errors in the measurements of HX rates do not, however, warrant the use of a more complex model.

3. On the basis of relative exchange energies, the measurable amide hydrogens of barstar can be divided into three groups:

- a) High energy (Group 1)
- b) Higher energy (Group 2)
- c) Highest energy (Group 3) (see Table I)

Of the measurable slow-exchanging amide hydrogens, the relative magnitude of  $\Delta G_{op}$  is smaller for the residues that form  $\beta$  strands 2 and 3 (Group 1). The  $\Delta G_{op}$  of *V45*, which forms the barnase-binding loop, is also comparable with the  $\beta$ -strand protons. The GdnHCl concentration-dependent exchange patterns for *V45* and *V50* (that forms the C-terminal  $\beta$ -strand) are illustrated in Figure 4A. Other measured  $\beta$ -sheet protons include *E52* and *I87*. The measured amide hydrogens

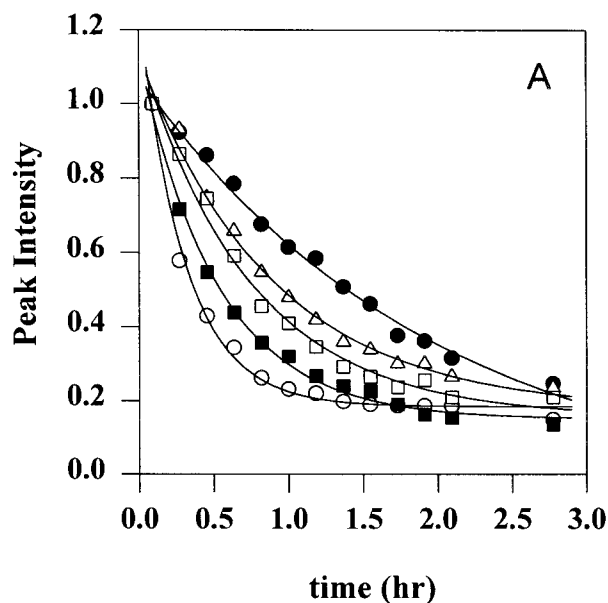
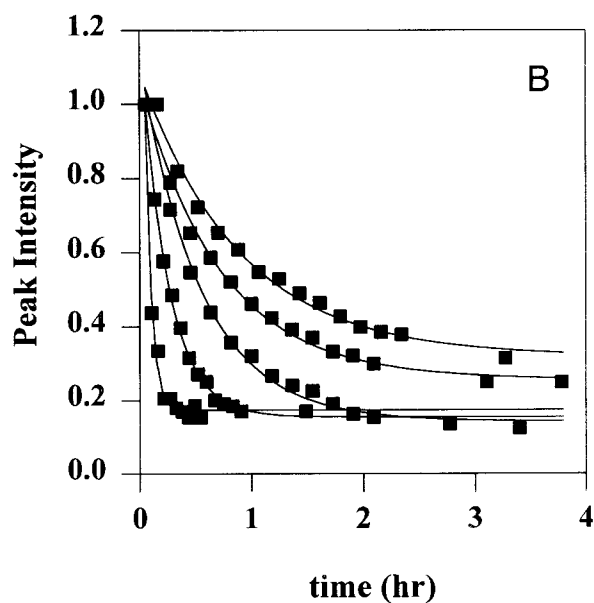


Fig. 2. **A**: Proton-to-deuterium exchange kinetics for the backbone amides of *L34* (○), *L49* (●), *V45* (△), *K78* (■), and *E8* (□) in the presence of 0.33 M GdnHCl in 20 mM phosphate buffer, pH 6.7, 32°C. The intensities were normalized with respect to the



intensity of the first spectrum. **B**: GdnHCl concentration-dependence of  $k_{\text{ex}}^{\text{obs}}$  for *K78*. The rates increase in the order: 0, 0.15, 0.33, 0.51, and 0.73 M GdnHCl.

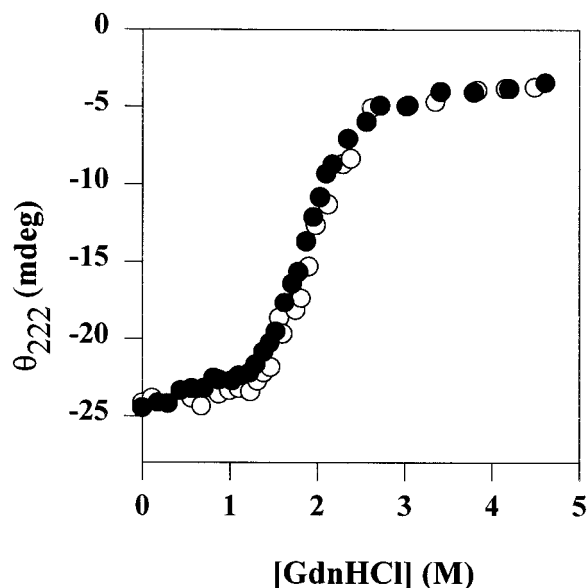


Fig. 3. Far-UV CD measurement of equilibrium unfolding [(●)  $\text{H}_2\text{O}$ , (○)  $\text{D}_2\text{O}$ ] at pH 7 to show the absence of any protein stabilizing effect of  $\text{D}_2\text{O}$ . In each case the data were fit to a two-state  $F \rightleftharpoons U$  model for unfolding as described earlier.<sup>29</sup>

from helices 1, 2, and 4 (*L16*, *E23*, *L34*, *D39*, *K78*), and the turn that connects  $\beta$ -strand 1 and helix 1 (*E8* and *R11*) have higher exchange energy (Group 2) than the  $\beta$ -sheet protons. In Figure 4B, the GdnHCl concentration-dependencies of  $\Delta G_{\text{op}}$  for *E8* and *R11* are shown.  $\Delta G_{\text{op}}$  values of these two residues, which belong to the helical turn preced-

ing helix 1, are largely degenerate. In Figure 4C the exchange behavior of two helical protons are illustrated: *L34* (helix 2) and *K78* (helix 4). The  $\Delta G_{\text{op}}$  of the amide hydrogen of *L49* (Fig. 4D) is the highest of all amide sites measured for barstar.  $\Delta G_{\text{op}}^{\circ}$  for *L49* in the native state of the protein is 6.7 kcal mol<sup>-1</sup>, higher than  $\Delta G_{\text{u}}^{\circ}$  (5.4 kcal mol<sup>-1</sup>) estimated from linear extrapolation of the global transition. The difference of 1.3 kcal mol<sup>-1</sup> is observed at all concentrations of GdnHCl higher than  $\sim 0.5$  M (Fig. 4D).

- Data for the exchange of the  $\epsilon_1\text{NH}$  of the indole side-chains of *W38* and *W44* are shown in Figure 5. In the calculation of their  $\Delta G_{\text{op}}$  values, the effect of neighboring side chains on the  $k_{\text{ch}}$  value was ignored (see footnote of Table I). The GdnHCl-dependent behavior of  $\Delta G_{\text{op}}$  for these two protons in the global part of the curve is identical with that for the Group 1 amide hydrogens.
- With an increase in GdnHCl concentration, the experimentally determined values of  $\Delta G_{\text{op}}$  for Group 1 amide protons as well as for the  $\epsilon_1\text{NH}$  of the indole side chains of *W38* and *W44* converge to zero at  $\approx 2.2$  M GdnHCl. For the Group 2 and Group 3 amide protons, the values of  $\Delta G_{\text{op}}$  converge to zero at  $\approx 2.6$  M GdnHCl. For all amide protons, the dependencies of the  $\Delta G_{\text{op}}$  values on GdnHCl concentration over the range 0 to 1.8 M, fit well to equation (12).
- By virtue of the lowest measured  $\Delta G_{\text{op}}$  values, only the Group 1 amide hydrogens (Table I) connect to the global transition energy at all

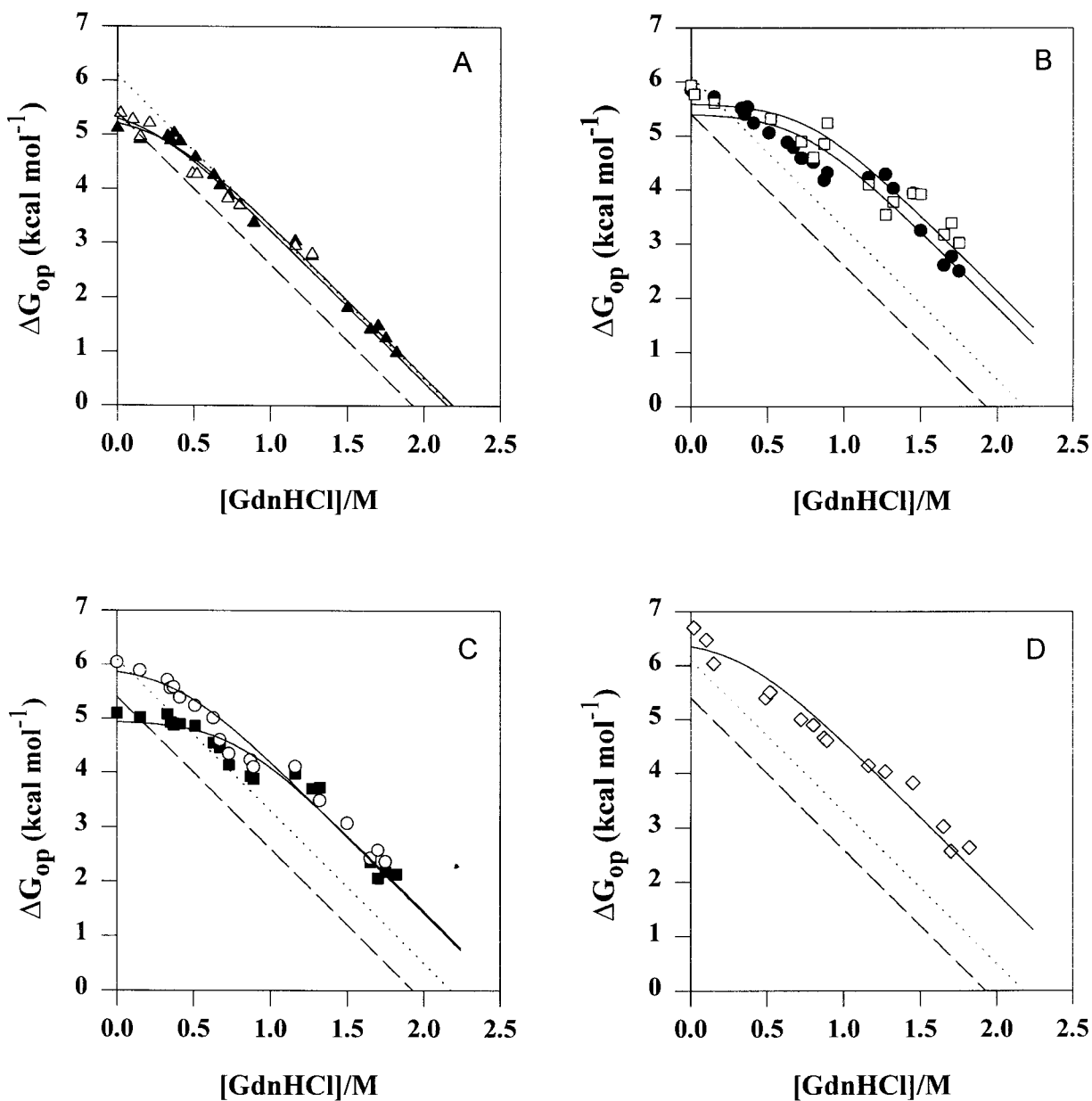


Fig. 4. GdnHCl concentration-dependence of free-energy of hydrogen exchange illustrated for a few protons. **A:** V45 ( $\blacktriangle$ ) and I87 ( $\triangle$ ). **B:** E8 ( $\bullet$ ) and R11 ( $\square$ ). **C:** L34 ( $\blacksquare$ ) and K78 ( $\circ$ ). **D:** L49 ( $\diamond$ ), the slowest of all measurable protons of barstar. The *dashed line* in each of the panels indicates the linearly extrapolated

free-energy of global unfolding of barstar. The *dotted line* (generated by adding  $0.7 \text{ kcal mol}^{-1}$  to the *dashed line* [eq. (11)] represents the global free energy of a transiently unfolded state where the *N*-aminoacyl bond of P48 exists in the native *cis* conformation (see the Discussion section).

GdnHCl concentrations beyond the pretransition region (Figure 4A). For Group 2 protons (Table I), the  $\Delta G_{op}$  values are consistently higher than the global unfolding energy at all GdnHCl concentrations measured. Group 3 (with highest exchange energy), consisting of L49 alone among the measurable residues, exchanges slower than the global rate at all GdnHCl concentrations down through the unfolding transition region.

In both the measurement of hydrogen exchange rates as a function of GdnHCl concentration and the measurement of stability from GdnHCl-induced equilibrium unfolding curves, no compensation was made for the variation in ionic strength due to the presence of varying concentrations of GdnHCl. A variation in the ionic strength during the measurement of hydrogen exchange rates by addition of KCl in the concentration range 0–0.8 M has, however, shown to have a

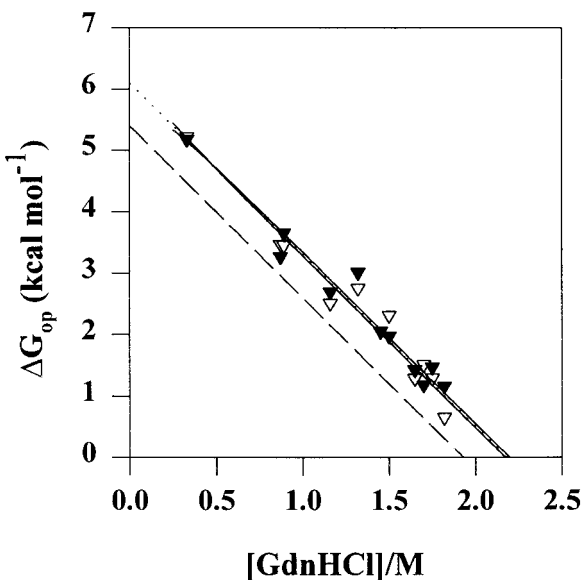


Fig. 5. GdnHCl-dependence of  $\Delta G_{op}$  for the  $\epsilon_1$ NH protons of W38 ( $\blacktriangledown$ ) and W44 ( $\triangledown$ ). As in Figure 4, the *dashed line* represents the unfolding free energy calculated from equilibrium experiments, while the *dotted line* shows the pertinent global free energy for HX of barstar.

negligible effect on the value of  $k_{ex}^{obs}$  (unpublished observations).

## DISCUSSION

### Exchange Rapidity of the Amide Hydrogens of Barstar

In this study, complete exchange of all measurable main-chain hydrogens in barstar was seen to occur in a few hours. This is probably because exchange was carried out at relatively high pH, and also because of the relatively low stability of barstar. Exchange studies could not be carried out at a lower pH because of solubility problems. Exchange can be dramatically slower under more acidic conditions, as seen from the HX rates for at least three other proteins. While the highest protection factor [eq. (5)] measured for an amide hydrogen of barstar is less than  $10^5$  (Table I), protection factors of up to  $10^9$  have been measured for other proteins. For oxidized cytochrome c, the typical exchange time for near-native states at  $30^\circ\text{C}$  is about 2 weeks,<sup>15</sup> and residual protection in 4.5 M GdnHCl-unfolded state has been observed for a few protons.<sup>33</sup> The C-terminal helical protons of reduced cytochrome c dissolved in 2.3 M GdnHCl,  $10^\circ\text{C}$  exchange at an average rate of  $0.082\text{ h}^{-1}$  (AKB, unpublished result). Even more interesting is a single crystal neutron diffraction study in which 28 amide hydrogens of ribonuclease A were found to be exchange-protected for  $\sim 1$  year.<sup>34</sup>

What structural factors enhance or retard hydrogen exchange in proteins is poorly understood. There has been an appreciable effort to correlate exchange

rates for various hydrogens with their location in the protein. It is generally believed that surface-exposed hydrogens and those forming flexible segments are fastest-exchanging, while hydrogens in secondary structural interfaces, involved in hydrogen bonding or buried in the protein interior, are slowest-exchanging (e.g., ref. 35). Such correlations do not always hold. For instance, several surface-exposed amide hydrogens of BPTI, which have been identified in the crystal structure to be hydrogen-bonded to surface water, exchange substantially slower than expected.<sup>36,37</sup> Recently, Eriksson and coworkers<sup>10</sup> have found that the lower base-catalyzed exchange rates for the surface-exposed residues originate from low water exposure of peptide carbonyls. Structural compactness and motions, which determine accessibility and concentration of  $\text{OH}^-$  ions at the site of exchangeable hydrogens, are also important factors that govern the rate of base-catalyzed rates. As evidenced by the extremely low enthalpy change and a relatively high heat capacity change during denaturation of barstar,<sup>29,32</sup> ring flip motions of *F74* in the hydrophobic core,<sup>21</sup> and cysteine modification with nitrobenzoate groups without major perturbation of the native structure,<sup>38</sup> barstar is structurally a highly flexible protein. This explains the rapid and complete exchange at the amide sites.

### The Two-State Process With Denaturant-Independent Local Exchange

It is fairly well established that two types of motions are responsible for hydrogen exchange in proteins: 1) small amplitude local fluctuations, and 2) large amplitude global unfolding motions. At a given pH, temperature, and denaturant concentration, the observed rate of exchange is the sum of exchange rates via local and global transitions. This defines the two-process model of hydrogen exchange.<sup>8,23,24,39</sup> The relative contributions of the two processes depend upon protein stability. Local fluctuations are largely responsible for exchange in higher stability regions, for example, at low denaturant concentration where the protein is natively like, and exchange via denaturational global motions dominates with increasing denaturant concentration. The HX model used in this study is based on the two-process behavior<sup>30</sup> with an ensemble of near-native exchange-competent states,  $N^*$ , existing in rapid equilibrium with  $N$ .

There are two basic assumptions of the model: 1) Under mildly destabilizing conditions there exists a rapid equilibrium between  $N$  and  $N^*$  such that HX behavior could be quantitatively treated in the EX2 limit; 2) the  $N \rightleftharpoons N^*$  equilibrium is only marginally sensitive to the presence of low concentrations of the denaturant. This latter assumption is based partly on empirical observations made here for barstar, and in other studies of oxidized cytochrome c,<sup>40</sup> ribonuclease A,<sup>14</sup> ribonuclease H,<sup>16</sup> and barnase.<sup>17</sup> Analogs of

$\Delta G_{op}$  curves like those in Figure 4 have also been calculated by using a statistical mechanical model developed for hydrogen exchange in globular proteins.<sup>41</sup> It should, however, be stressed here that little is known about how local motions in proteins are affected by mildly destabilizing conditions. Indeed, HX methods in conjunction with NMR offer a means to study conformational fluctuations under stabilizing conditions.

Is there only one unique  $N^*$  state for each exchangeable hydrogen? It has been proposed that a fully folded protein has a rough energy surface comprising a large number of conformational substates.<sup>42–45</sup> Recent experimental observation of conformational fluctuations in real time lends support to the reality of such ruggedness.<sup>46</sup> It remains to be shown whether an  $N^*$  state can be identified with a conformational substate. A proton can be exchange-competent in more than one near-native state, for example, when the amide site stays solvent-exposed in two or more energy-disparate substates. Thus, several fluctuational equilibria may be included in the expression for the observed exchange rate,

$$k_{ex}^{obs} = [\sum K_{1,i} + K_{1,i}K_{2,i}]k_{ch} \quad (14)$$

where  $I$  refers to a particular  $N^*$  state in rapid equilibrium with  $N$ .

### Validity of the EX<sub>2</sub> Assumption

The validity of the EX<sub>2</sub> mechanism for HX of any protein is confirmed typically by determining the pH dependence of  $k_{ex}^{obs}$ , but this was not possible for barstar because exchange is too fast above pH 7, and the low solubility of barstar below pH 6.5 precludes measurements at lower pH. Although proteins undergo hydrogen exchange usually by the EX<sub>2</sub> mechanism in native-like conditions, high temperature, moderate to high concentrations of denaturants or pH values above 7 may cause the exchange mechanism to change from EX<sub>2</sub> to EX<sub>1</sub>.<sup>13</sup> It was therefore important to confirm the validity of the EX<sub>2</sub> mechanism in the conditions used for HX in this study. In particular, the two-process model depicted in equation (2) and its mathematical development to equation (12) are based on the assumption that the EX<sub>2</sub> mechanism is valid over the entire range (0 to 1.8 M) of GdnHCl concentration studied.

The important criterion for the EX<sub>2</sub> mechanism of exchange is that  $k_{cl}$  be much larger in value than  $k_{ch}$  [eq. (4)]. For the set of amide hydrogens studied here at pH 6.7 and 32°C, the largest value of  $k_{ch}$  is 9 s<sup>-1</sup> (Table I), and  $k_{cl}$  must therefore be much larger than 9 s<sup>-1</sup> over the entire range of GdnHCl studied. Three kinetic phases of folding have been described for barstar. Phase 0 is complete in the submillisecond time domain for all concentrations of denaturant used in this study.<sup>47,48</sup> Phase 2 occurs with a rate that decreases from 34 s<sup>-1</sup> in water to 6 s<sup>-1</sup> in 1.8 M

GdnHCl, while phase 1 occurs at a rate of 0.008 s<sup>-1</sup>. Clearly, if it is structure formation in kinetic phases 2 or 1 that affords protection from exchange, the mechanism for exchange cannot be EX<sub>2</sub>. Only if structure formation in phase 0 is responsible for protection from exchange will the EX<sub>2</sub> mechanism be valid.

Two experimental observations attest to the validity of the use of the EX<sub>2</sub> mechanism in the present study. These observations were made possible because stopped-flow NMR measurement of hydrogen exchange allowed the range of GdnHCl concentration to be extended to as high as 1.8 M, which is only slightly lower than the midpoint of the equilibrium unfolding transition. First, according to equation (13), the value of  $\Delta G_{op}$  for each amide hydrogen must converge to 0 at the midpoint of the global unfolding transition. This is observed (Fig. 4). Second, the slope of the linear dependence of  $\Delta G_{op}$  on GdnHCl concentration must be given by  $m$ , which is also the slope of the linear dependence of  $\Delta G_u$  on GdnHCl concentration [eq. (11)]. This too is observed in Figure 4. The second point is particularly important because if the mechanism had changed from EX<sub>2</sub> to EX<sub>1</sub> in the transition zone of global unfolding, then the slope of the observed linear dependence of  $\ln k_{ex}^{obs}/k_{ch}$  on GdnHCl would change from that of the linear dependence of  $\ln K_{op}$  on GdnHCl concentration to that of the linear dependence of  $\ln k_{cl}$  on GdnHCl concentration. The latter slope is significantly less than the former slope.<sup>49</sup>

### $\Delta G_{op}$ vs $\Delta G_u$

The observation that  $\Delta G_{op}^{\circ}$  for many amide hydrogens is significantly larger than  $\Delta G_u^{\circ}$  (Fig. 4 and Table I) is surprising. If the transiently unfolded  $U^*$  state that is exchange competent in strongly native-like conditions [see eq. (2)] is structurally and energetically identical to the equilibrium unfolded state,  $U$ , that forms in high concentrations of GdnHCl, then equations (6), (7), and (8) demand that  $K_u \leq K_{op}$ , and the value of  $\Delta G_{op}$  may therefore be less than that of  $\Delta G_u$  but not larger. It is, however, important to note that unlike equilibrium unfolding experiments, HX is a kinetic measurement, much like a double-jump experiment where the exchanging unfolded state gets little time to relax. Consequently,  $\Delta G_{op}$  equals the energy difference between the native and the  $U^*$  state, which is kinetically accessible in the HX time scale. If this unrelaxed  $U^*$  state is higher in energy than the equilibrium  $U$  state, then it is possible for  $\Delta G_{op}$  to be larger than  $\Delta G_u$ .

A possible explanation for the exchange-competent transiently unfolded  $U^*$  state [eq. (2)] being less stable than the equilibrium unfolded  $U$  state is based on the following three-state kinetic mechanism for unfolding, which has been shown to be operative at denaturant concentration higher than

~1.9 M, which is the  $C_m$  for barstar<sup>50</sup>:



$U_F$  (fast refolding) and  $U_S$  (slow refolding) forms are assumed to contain the *Y47-P48* bond in the native cis and the nonnative trans conformation, respectively.<sup>51</sup> On unfolding  $U_F$  is first formed, and it slowly converts to  $U_S$ . The rate constant for the  $U_F \rightarrow U_S$  reaction is 40 hr<sup>-1</sup>, much slower than  $k_{ch}$  values, which rate-limit hydrogen exchange under EX2 conditions (Table I). Thus, in the context of hydrogen exchange, the  $U^*$  state of equation (2) can be taken as  $U_F$ , but in an equilibrium unfolding experiment the properties of the  $U$  state arise from an equilibrium mixture of  $U_F$  and  $U_S$ . The free-energy of  $U_F$  is higher than that for  $U_S$ , meaning that  $\Delta G_{op}$  measures the energy difference between  $N$  and  $U_F$ , whereas  $\Delta G_u$  measures the energy difference between  $N$  and an equilibrium mixture of  $U_F$  and  $U_S$ .  $\Delta\Delta G$ , the difference between  $\Delta G_{op}$  and  $\Delta G_u$  for barstar will then be

$$\Delta\Delta G = -RT \ln \frac{K_{21}}{1 + K_{21}}. \quad (16)$$

With  $K_{21} = U_F/U_S = 0.47$ ,<sup>50</sup> the proline-related energy difference is ~0.7 kcal mol<sup>-1</sup>. Addition of 0.7 kcal mol<sup>-1</sup> to  $\Delta G_u$  produces the dotted line shown in Figure 4.

This correction makes  $\Delta G_u$  consistent with  $\Delta G_{op}$  for the Group 1 (high  $\Delta G_{op}$ ) amide protons and the indole  $\epsilon_1$ NH only (Fig. 4).  $\Delta G_{op}$  values for Group 2 amide hydrogens along with the amide hydrogen of *L49* still stay higher than  $\Delta G_u$  by ~0.35–0.65 kcal mol<sup>-1</sup> throughout the global transition region (Fig. 4B–D). There are several possible explanations:

1. Residual structure is present in the exchange-competent transiently unfolded state,  $U^*$ , which involves Groups 2 and 3 amide hydrogens (but not Group 1 amide hydrogens). Residual structure would imply that the values for  $k_{ch}$  used in equation (5) for Groups 2 and 3 residues (Table I), which were calculated on the basis of poly-DL-alanine reference rates, are overestimates for the actual chemical exchange rates. An overestimation of  $k_{ch}$  would result in higher  $\Delta G_{op}$ . It is interesting to note that the calculated  $k_{ch}$  values for Group 2 residues (except *L16*) are at least threefold larger than the calculated  $k_{ch}$  values for Group 1 residues (Table I), which are present in either the hydrophobic core or in hydrophobic clusters in the  $N$  state (see below). It should also be mentioned that in equation (2),  $k_{ch}^1$  has also been assumed to be equal to  $k_{ch}^2$ .
2. Recent stopped-flow CD measurements of the unfolding of barstar have revealed the presence of a transient unfolding intermediate,  $I_U$ , on the

unfolding pathway.<sup>52</sup> A large fraction of the secondary structure is missing in  $I_U$ , which nevertheless appears to have an intact hydrophobic core. It has been shown that  $I_u$  is less stable than  $U_F$ . The large loss of secondary structure in  $I_u$  makes it an unlikely candidate for  $N^*$ , which is the product of local unfolding events, but it is possible that it represents the exchange-competent  $U^*$  state for Groups 2 and 3 amide protons. The mechanism in equation (2) demands that  $U^*$  form rapidly from  $N$  and convert relatively slowly to  $U$ .  $I_U$  possesses these properties. Thus, the  $U^*$  state in equation (2) might correspond to the  $U_F$  state for Group 1 amide hydrogens and the  $I_U$  state for Groups 2 and 3 amide protons. Pulsed amide hydrogen exchange studies of the unfolding pathway of barstar, which are currently in progress, will indicate whether Group 1 amide protons are indeed protected from exchange in  $I_u$ , whereas Groups 2 and 3 amide protons are not.

3. In native barstar the *N*-aminoacyl bond of *P27* exists in the trans conformation.<sup>20</sup> It is not known if the trans conformation is retained in equilibrium unfolded protein. If it is not completely retained, a correction similar to that described above for isomerization at the *Y47-P48* peptide bond would be necessary.
4. The assumptions made in the analysis [eq. (2)] may not be correct.

Proline-dependent  $U_F$  and  $U_S$  forms are known for several other proteins, including ribonuclease A,<sup>53,54</sup> and oxidized cytochrome c.<sup>55</sup> For both oxidized cytochrome c<sup>9,15</sup> and ribonuclease A,<sup>14</sup>  $\Delta G_{op}$  values for a few of the slowest exchanging amides are greater than the  $\Delta G_u$  value estimated from equilibrium unfolding experiments, similar to what is seen here for the Groups 2 and 3 amide hydrogens. In the case of oxidized cytochrome c, it was proposed that these amide hydrogens were involved in residual structure in the unfolded state.<sup>9</sup> The discrepancy observed for ribonuclease A becomes small when the  $\Delta G_u$  value estimated from calorimetric melting data is compared with  $\Delta G_{op}$ , and becomes smaller when the free energy of cis  $\rightleftharpoons$  trans equilibria of proline isomers in the unfolded polypeptide is taken into account.<sup>15</sup> It is emphasized that the  $\Delta G_u$  values for barstar obtained calorimetrically or by using optical techniques, as here, are identical<sup>32</sup> and that the stability of the protein in H<sub>2</sub>O and D<sub>2</sub>O solutions is the same.

### Hydrogen Exchange Pattern, Backbone Dynamics and Folding Domains of Barstar

In the NMR structure, the residues constituting the set of high exchange energy protons (Group 1) are more or less shielded from the solvent. The NH of *V45* is hydrogen bonded to the CO of *C40*. *V45* is located in the barnase binding loop and forms part of the hydrophobic core of barstar. *V50* and *I87*, which

**TABLE I. Hydrogen Exchange Properties and Spatial Location of Some Measured Amide Protons of Barstar in the Absence of GdnHCl**

Residue	Surface accessibility (%) <sup>*</sup>	Spatial location/ structure <sup>*</sup>	$k_{\text{ex}}^{\text{obs} \dagger}$ (h <sup>-1</sup> )	$k_{\text{ch}}^{\ddagger}$ (h <sup>-1</sup> )	$P^{\S}$	$\Delta G_{\text{op}}^{\P}$ (kcal/mol)
<i>Group 1</i> (residues for which $\Delta G_{\text{op}} \approx \Delta G_{\text{u}}$ )						
V45	8	Barnase binding loop, between helix 2 and $\beta$ -strand 2	0.90	4,000	4,400	5.1
V50	19	$\beta$ -strand 2; the aliphatic protons make contact with E52 and T85	0.70	3,000	4,200	5.1
E52	21	$\beta$ -strand 2; packs onto V4	1.48	5,000	3,300	4.9
I87	34	$\beta$ -strand 3	0.40	2,900	7,200	5.4
<i>Group 2</i> (residues for which $\Delta G_{\text{op}} > \Delta G_{\text{u}}$ )						
E8	63	Helical turn between $\beta$ -strand 1 and helix 1	0.78	12,000	15,300	5.8
R11	79	Extended loop before helix 1	1.05	18,700	17,800	5.9
L16	0	Helix 1	1.62	4,600	2,800	4.8
E23	22	Helix 1	2.25	10,700	4,700	5.1
L34	23	Helix 2	4.64	14,500	3,100	4.9
D39	76	Helix 2	3.12	10,000	3,200	4.9
Q72	43	Helix 4	2.28	18,700	8,200	5.5
K78	38	Helix 4	1.12	24,000	21,400	6.0
<i>Group 3</i> (the slowest-exchanging residue with $\Delta G_{\text{op}} > \Delta G_{\text{u}}$ )						
L49	1	$\beta$ -strand 2; the NH donates a hydrogen bond to CO of D83	0.42	27,700	65,900	6.7
<i>Indole amides<sup>¶</sup></i>						
W38	20	Helix 2	1.0	5,220	5,220	5.14
W44	50	Loop between helix 2 and $\beta$ -strand 2	0.94	5,220	5,550	5.20

<sup>\*</sup>From reference 21, with permission.

<sup>†</sup> $k_{\text{ex}}^{\text{obs}}$ , observed exchange rates in the absence of GdnHCl

<sup>‡</sup> $k_{\text{ch}}$  values at 32°C, pH 7.1 (after correcting for glass electrode reading) were calculated using poly-DL-alanine reference rates published for 20°C.<sup>25</sup> To compensate for the temperature offset, the activation energy suggested by the authors (18 kcal mol<sup>-1</sup> for base catalysis) was used. In the present experimental conditions, water- and acid-catalysis are negligible. The numbers shown are base-catalyzed rates. The effect of side chains of the left and the right neighboring residue was ignored in calculating the  $k_{\text{ch}}$  value for the tryptophan indole amide.

<sup>§</sup>The ratio of  $k_{\text{ch}}$  to  $k_{\text{ex}}^{\text{obs}}$

<sup>¶</sup>The values for  $\Delta G_{\text{op}}$  may be compared against  $\Delta G_{\text{u}}^{\circ} = 5.4$  kcal mol<sup>-1</sup> (6.1 kcal mol<sup>-1</sup> after introducing the proline-related correction, see text)

<sup>||</sup>Values for  $k_{\text{ex}}^{\text{obs}}$ ,  $k_{\text{ch}}$ , and  $\Delta G_{\text{op}}$  are given for 0.33 M GdnHCl.

form  $\beta$  strands 2 and 3, respectively, are relatively exposed on the surface. Their aliphatic side chains are part of hydrophobic clusters on the outside of the protein.<sup>21</sup> Of the set of higher  $\Delta G_{\text{op}}$  amide hydrogens (Group 2), L16, E23, L34, and K78 are part of helix 1, 1, 2, and 4, respectively. While their amide protons are hydrogen bonded, the side chains form the hydrophobic core. E52 is in the middle of  $\beta$ -strand 2, and its side chain packs onto V4. E8 and R11 form the turn between  $\beta$ -strand 1 and helix 1. This turn, supported by a hydrogen bond between NH of I10 and the CO of G7 and/or N6, must be rigid enough to slow down the exchange of E8 and R11. I10 has been

reported to be protected from exchange.<sup>20</sup> L49, the amide hydrogen of which exchanges slowest, is the first residue of  $\beta$ -strand 2. The retardation of the hydrogen exchange rate for L49 is distinctly noticeable (Table I). A protection factor of  $\sim 6.6 \times 10^4$ , the largest among the measured residues, can be strongly correlated with the H-bond donated by the NH of L49 to the CO of D83, the first residue of  $\beta$ -strand 3. Besides slowing down the exchange of L49 enormously ( $\Delta G_{\text{op}}$  is higher than the corrected  $\Delta G_{\text{u}}$  by  $\sim 0.7$  kcal mol<sup>-1</sup> at all guanidine concentrations), the hydrogen bond most likely stabilizes the association of  $\beta$  strands 2 and 3 (Fig. 6).

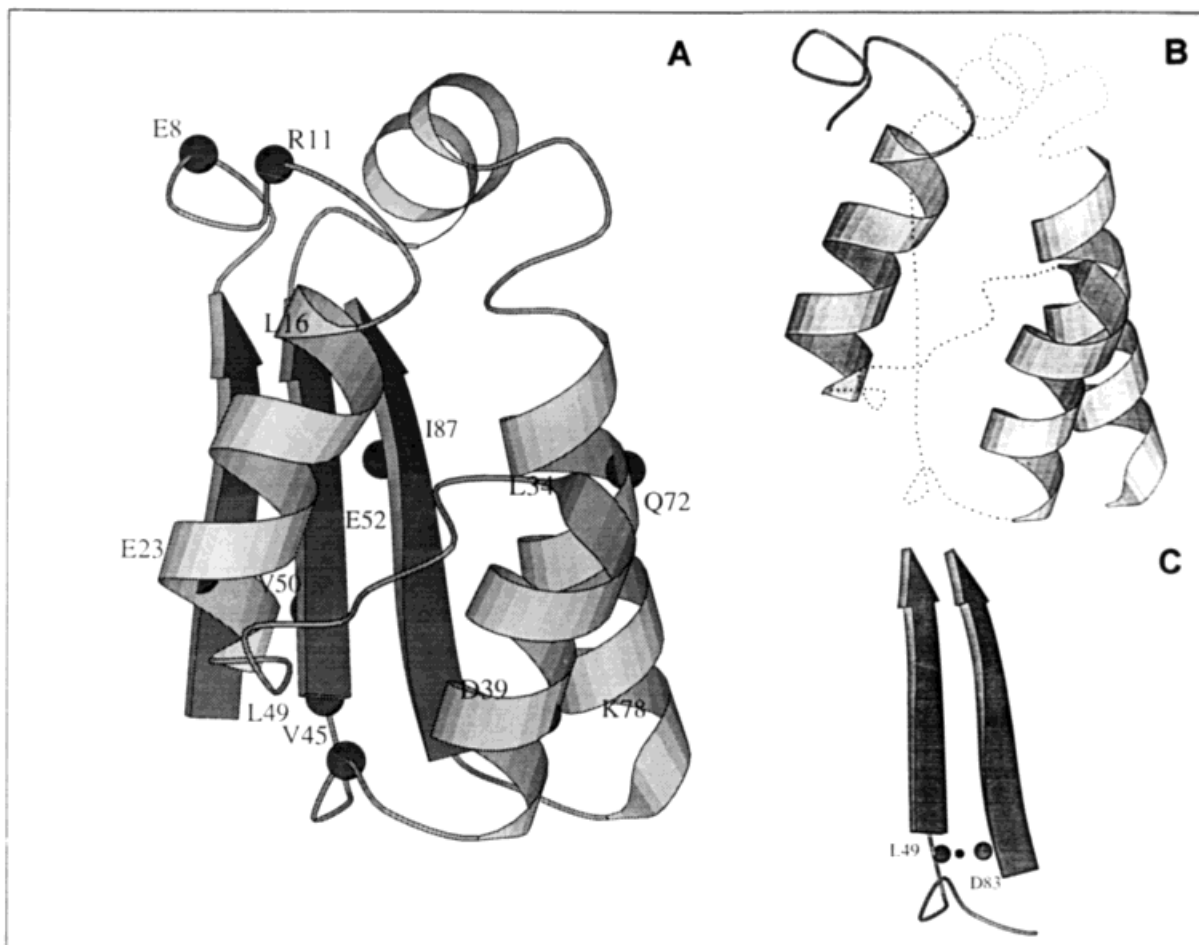


Fig. 6. **A:** Ribbon diagram of barstar based on the NMR solution structure.<sup>21</sup> Residues used for main-chain hydrogen exchange measurement are shown explicitly. **B:** Helices 1, 2, and 4, and the turn formed of *E8* and *R11*. **C:** The domain formed of  $\beta$

strands 2 and 3 along with the barnase binding loop. Also shown in this panel is *L49* and the hydrogen bond that its NH donates to the CO of *D83*. This figure was prepared using MOLSCRIPT.<sup>56</sup> PDB file: 1BTA.

From the exchange pattern of observable amides of barstar, two structural subdomains can be identified (Fig. 6). One, for which  $\Delta G_{op} \approx \Delta G_u$  (Group 1 protons, see Table I), is formed from the association of  $\beta$  strands 2 and 3. The other domain is defined by the parallel helix bundle formed of helices 1, 2, and 4. The amide hydrogens of Group 2 for which  $\Delta G_{op}$  is larger than  $\Delta G_u$  form this domain. The slower exchange behavior of the amide hydrogens of this domain observed here is consistent with the report of Fersht and coworkers<sup>20</sup> who noted significant exchange protection of amide protons of helices 1, 2, and 4. The two domains are shown in Figure 6.

The two structural subdomains of barstar can also be distinguished on the basis of backbone relaxation and segmental mobility. A  $^1\text{H}$ -detected  $^{15}\text{N}$  nuclear spin relaxation study of barstar (manuscript submitted for publication) has identified domain 2 with low-frequency conformational exchanging motions, in addition to picosecond range internal motions,

occurring in the microsecond or slower time scale. On the other hand,  $T_2$  relaxation data for residues forming  $\beta$  strands 2 and 3 could be modeled without adding slow motional terms, suggesting relative rigidity of domain 2.

The relevance of structural subdomains in a protein, which have been identified by equilibrium studies as reported here for barstar, to the direct kinetic folding pathway of the protein is still controversial. Based on isoenergetic HX behavior in the preglobular region for various spatially located residues, three subglobal folding units were identified for the oxidized state of cytochrome *c*.<sup>9,40</sup> Englander and coworkers<sup>9,40</sup> hold that these subglobal units represent steps in a kinetic unfolding sequence. On the other hand, the partly unfolded form of barnase that has been identified by equilibrium HX studies is not similar structurally to the partly folded kinetic intermediate.<sup>17</sup> In the case of barstar, the inability to measure hydrogen exchange rates for a large num-

ber of residues does not permit an extensive analysis in terms of the partially unfolded forms. It remains to be seen if the two subdomains identified here, indeed, represent intermediates on the (un)folding pathway of barstar.

#### ACKNOWLEDGMENTS

The NMR spectra were recorded in the National Facility for High Resolution NMR, TIFR, Mumbai, supported by the Department of Science and Technology, Government of India. We thank Prof. R.L. Baldwin and Dr. Raghavan Varadarajan for discussion and comments on the manuscript.

#### REFERENCES

1. Englander, S.W., Kallenbach, N.R. Hydrogen exchange and structural dynamics of proteins and nucleic acids. *Q. Rev. Biophys.* 16:521-655, 1984.
2. Udgaonkar, J.B., Baldwin, R.L. NMR evidence for an early framework intermediate on the folding pathway of ribonuclease A. *Nature* 335:694-699, 1988.
3. Roder, H., Elöve, G.A., Englander, S.W. Structural characterization of folding intermediates in cytochrome c by H-exchange labelling and proton NMR. *Nature* 335:700-704, 1988.
4. Englander, S.W., Mayne, L. Protein folding studied using hydrogen-exchange labeling and two-dimensional NMR. *Annu. Rev. Biophys. Biomol. Struct.* 21:243-265, 1992.
5. Baum, J., Dobson, C., Evans, P., Hanley, C. Characterization of a partly folded protein by NMR methods: Studies on the molten globule state of guinea pig  $\alpha$ -lactalbumin. *Biochemistry* 28:7-13, 1989.
6. Englander, S.W., Englander, J.J., McKinnie, R., Ackers, G.K., Turner, G.J., Westrick, J.A., Gill, S.J. Hydrogen exchange measurement of the free energy of structural and allosteric change in hemoglobin. *Science* 256:1684-1687, 1992.
7. Kim, K.-S., Fuchs, J.A., Woodward, C.K. Hydrogen exchange identifies native-state motional dynamics important in protein folding. *Biochemistry* 32:9600-9608, 1993.
8. Kim, K.-S., Woodward, C. Protein internal flexibility and global stability: Effect of urea on hydrogen exchange rates of bovine pancreatic trypsin inhibitor. *Biochemistry* 32:9609-9613, 1993.
9. Bai, Y., Sosnick, T.R., Mayne, L., Englander, S.W. Protein folding intermediates: Native state hydrogen exchange. *Science* 269:192-196, 1995.
10. Eriksson, M.A.L., Härd, T., Nilsson, L. On the pH dependence of amide proton exchange rates in proteins. *Biophys. J.* 69:329-339, 1995.
11. Perrett, S., Clarke, J., Hounslow, A.M., Fersht, A.R. Relationship between equilibrium amide proton exchange behavior and the folding pathway of barnase. *Biochemistry* 34:9288-9298, 1995.
12. Christoffersen, M., Bolvig, S., Tüchsen, E. Salt effects on the amide hydrogen exchange of bovine pancreatic trypsin inhibitor. *Biochemistry* 35:2309-2315, 1996.
13. Loh, S.N., Rohl, C.A., Kiefhaber, T., Baldwin, R.L. A general two-process model describes the hydrogen exchange behavior of RNase A in unfolding conditions. *Proc. Natl. Acad. Sci. U.S.A.* 93:1982-1987, 1996.
14. Mayo, S.L., Baldwin, R.L. Guanidinium chloride induction of partial unfolding in amide proton exchange in RNase A. *Science* 262:873-876, 1993.
15. Bai, Y., Milne, J.S., Mayne, L., Englander, S.W. Protein stability parameters measured by hydrogen exchange. *Proteins* 20:4-14, 1994.
16. Chamberlain, A.K., Handel, T.M., Marqusee, S. Detection of rare partially folded molecules in equilibrium with the native conformation of RNaseH. *Nature Struct. Biol.* 3:782-787, 1996.
17. Clarke, J., Fersht, A.R. An evaluation of the use of hydrogen exchange at equilibrium to probe intermediates on the protein folding pathway. *Folding Design* 1:243-254, 1996.
18. Hartley, R.W. Barnase and barstar. Expression of its cloned inhibitor permits expression of a cloned ribonuclease. *J. Mol. Biol.* 202:913-915, 1988.
19. Nath, U., Udgaonkar, J.B. How do proteins fold? *Curr. Sci.* 72:180-191, 1997.
20. Lubienski, M.J., Bycroft, M., Jones, D.N.M., Fersht, A.R. Assignment of the backbone  $^1\text{H}$  and  $^{15}\text{N}$  NMR resonance and secondary structure characterization of barstar. *FEBS Lett.* 332:81-87, 1993.
21. Lubienski, M.J., Bycroft, M., Freund, S.M.V., Fersht, A.R. Three-dimensional solution structure and  $^{13}\text{C}$  assignments of barstar using nuclear magnetic resonance spectroscopy. *Biochemistry* 33:8866-8877, 1994.
22. Khurana, R., Udgaonkar, J.B. Equilibrium unfolding studies of barstar: Evidence for an alternative conformation which resembles a molten globule. *Biochemistry* 33:106-115, 1994.
23. Woodward, C.K., Rosenberg, A. Studies of hydrogen exchange in proteins. VI. Urea effects on ribonuclease exchange kinetics leading to a general model for hydrogen exchange from folded proteins. *J. Biol. Chem.* 246:4114-4121, 1971.
24. Woodward, C.K., Hilton, B.D. Hydrogen isotope exchange kinetics of single protons in bovine pancreatic trypsin inhibitor. *Biophys. J.* 32:561-575, 1980.
25. Bai, Y., Milne, J.S., Mayne, L., Englander, S.W. Primary structure effects on peptide group hydrogen exchange. *Proteins* 17:75-86, 1993.
26. Hvidt, A. A discussion of the pH dependence of the hydrogen-deuterium exchange of proteins. *C. R. Trav. Lab. Carlsberg* 34:299-317, 1964.
27. Pace, C.N. The stability of globular proteins. *CRC Crit. Rev. Biochem.* 3:1-43, 1975.
28. Myers, J.K., Pace, C.N., Scholtz, J.M. Denaturant  $m$  values and heat capacity changes: Relation to changes in accessible surface areas of protein unfolding. *Protein Sci.* 4:2138-2148, 1995.
29. Agashe, V.R., Udgaonkar, J.B. Thermodynamics of denaturation of barstar: Evidence for cold denaturation and evaluation of the interaction with guanidine hydrochloride. *Biochemistry* 34:3286-3299, 1995.
30. Qian, H., Mayo, S.L., Morton, A. Protein hydrogen exchange in denaturant: Quantitative analysis by a two-process model. *Biochemistry* 33:8167-8171, 1994.
31. Khurana, R., Hate, A.T., Nath, U., Udgaonkar, J.B. pH dependence of the stability of barstar to chemical and thermal denaturation. *Protein Sci.* 4:1133-1144, 1995.
32. Wintrode, P.L., Griko, Y.V., Privalov, P.L. Structural energetics of barstar studied by differential scanning microcalorimetry. *Protein Sci.* 4:1528-1534, 1995.
33. Elöve, G.A., Bhuyan, A.K., Roder, H. Kinetic mechanism of cytochrome c folding: Involvement of the heme and its ligands. *Biochemistry* 33:6925-6935, 1994.
34. Wlodawer, E., Sjölin, L. Hydrogen exchange in RNase: Neutron diffraction study. *Proc. Natl. Acad. Sci. U.S.A.* 79:1418-1422, 1982.
35. Gregory, R.B., Rosenberg, A. Protein conformational dynamics measured by hydrogen isotope exchange techniques. *Methods Enzymol.* 131:448-508, 1986.
36. Tüchsen, E., Woodward, C. Hydrogen kinetics of peptide amide protons at the bovine pancreatic trypsin inhibitor protein-solvent interface. *J. Mol. Biol.* 185:405-419, 1985.
37. Tüchsen, E., Woodward, C. Mechanism of surface peptide proton exchange in bovine pancreatic trypsin inhibitor: Salt effects and  $O$ -protonation. *J. Mol. Biol.* 185:421-430, 1985.
38. Ramachandran, S., Udgaonkar, J.B. Stabilization of barstar by chemical modification of the buried cysteines. *Biochemistry* 35:8776-8785, 1996.
39. Woodward, C., Simon, I., Tüchsen, E. Hydrogen exchange and the dynamic structure of proteins. *Mol. Cell. Biochem.* 48:135-160, 1982.

40. Bai, Y., Englander, S.W. Future directions in folding: The multi-state nature of protein structure. *Proteins* 24:145–151, 1996.
41. Miller, D.W., Dill, K.A. A statistical mechanical model for hydrogen exchange in globular proteins. *Protein Sci.* 4: 1860–1873, 1996.
42. Bryngelson, J.D., Wolynes, P.G. Spin glasses and the statistical mechanics of protein folding. *Proc. Natl. Acad. Sci. U.S.A.* 84:7524–7528, 1987.
43. Bryngelson, J.D., Wolynes, P.G. Intermediates and barrier crossing in a random energy model (with applications to protein folding). *J. Phys. Chem.* 93:6902–6915, 1989.
44. Dill, K.A., Bromberg, S., Yue, K., Fiebig, K.M., Yee, D.P., Thomas, P.D., Chan, H.S. Principles of protein folding: A perspective from simple exact models. *Protein Sci.* 4:561–602, 1995.
45. Wolynes, P.G., Onuchic, J.N., Thirumalai, D. Navigating the folding routes. *Science* 267:5204–5205, 1995.
46. Leeson, D.T., Wiersma, D.A. Looking into the energy landscape of myoglobin. *Nature Struct. Biol.* 2:848–851, 1995.
47. Nölting, B., Golbik, R., Fersht, A.R. Submillisecond events in protein folding. *Proc. Natl. Acad. Sci. U.S.A.* 92:10668–10672, 1997.
48. Nath, U., Udgaonkar, J.B. Folding of trypsin mutant of barstar: Evidence for an initial hydrophobic collapse on the folding pathway. *Biochemistry* 36:8602–8610, 1997.
49. Shastry, M.C.R., Udgaonkar, J.B. The folding mechanism of barstar: Evidence for multiple pathways and multiple intermediates. *J. Mol. Biol.* 247:1013–1027, 1995.
50. Shastry, M.C.R., Agashe, V.R., Udgaonkar, J.B. Quantitative analysis of the kinetics of denaturation and renaturation of barstar in the folding transition zone. *Protein Sci.* 3:1409–1417, 1994.
51. Schreiber, G., Fersht, A.R. The refolding of cis- and trans-peptidylprolyl isomers of barstar. *Biochemistry* 32:11195–11203, 1993.
52. Nath, U., Agashe, V.R., Udgaonkar, J.B. Initial loss of secondary structure in the unfolding of barstar. *Nature Struct. Biol.* 3:920–923, 1996.
53. Garel, J.-R., Baldwin, R.L. Both the fast and the slow refolding reactions of ribonuclease A yield native enzyme. *Proc. Natl. Acad. Sci. U.S.A.* 70:3347–3350, 1973.
54. Schmid, F.X. Proline isomerization in unfolded ribonuclease A. *Eur. J. Biochem.* 128:77–80, 1982.
55. Nall, B. Proline isomerization and protein folding. *Mol. Cell Biophys.* 3:123–143, 1985.
56. Kraulis, P.J. (1991) "MOLSCRIPT: A program to produce both detailed and schematic plots of protein structures." *J. Appl. Crystallogr.* 24:946–950, 1991.